Taylor & Francis
Taylor & Francis Group

Spectroscopy Letters

An International Journal for Rapid Communication

ISSN: 0038-7010 (Print) 1532-2289 (Online) Journal homepage: http://www.tandfonline.com/loi/lstl20

Coal Exploration Technology Based on Visible-Infrared Spectra and Remote Sensing Data

Ba Tuan Le, Dong Xiao, Desmond Okello, Dakuo He, Jialiu Xu & Trung Thanh Doan

To cite this article: Ba Tuan Le, Dong Xiao, Desmond Okello, Dakuo He, Jialiu Xu & Trung Thanh Doan (2017): Coal Exploration Technology Based on Visible-Infrared Spectra and Remote Sensing Data, Spectroscopy Letters, DOI: 10.1080/00387010.2017.1354889

To link to this article: http://dx.doi.org/10.1080/00387010.2017.1354889

Coal Exploration Technology Based on Visible-Infrared Spectra and Remote Sensing Data

Ba Tuan Le[1,2], Dong Xiao[1,*], Desmond Okello[3], Dakuo He[1], Jialiu Xu[1], Trung Thanh Doan[2]
[1]Information Science and Engineering School, Northeastern University, Shenyang, China
[2]Control Technology College, Le Quy Don Technical University, Hanoi, Vietnam
[3]Department of Software College, Northeastern University, Shenyang, China

Corresponding author Dong Xiao E-mail: xiaodong@ise.neu.edu.cn

Abstract

In the modern society, coal is used as the main source of energy. In this paper, based on the theory of the remote sensing, the distributions of the coal mine area through the satellite imagery are measured. Firstly, the satellite pictures of coal mining regions in Quangninh of Vietnam and Huolinhe of China were gathered as the experimental data. Secondly, spectrometer was used to measure the spectral data of the coal samples of these two regions. The measured data provides comprehensive and accurate spectral characteristics of the coal. Then the classification model can be built by the improved Extreme Learning Machines algorithm based on the measured data and the remote sensing data. Finally, the distribution image of the coal mine area is obtained accurately based on the classification model.

KEYWORDS: Remote Sensing; Coal; Visible-Infrared Spectra; Extreme Learning Machines

1. INTRODUCTION

Remote sensing is the acquisition of information about an object or phenomenon without making a physical contact with the object, which is widely used in numerous fields [1-3]. Plenty of studies have shown that the remote sensing technology is an effective way in the coal research, exploration and measurement, which has been used in the mining field since the 1970s [4-6] and plays an important role in the field of the coal mine detection. This method extracts and analyzes the reflection information based on the various features of the reflection spectrum response in order to identify the characteristics of the different features, judge the measured area geology and finally find the coal mine area.

Based on the multiple remote sensing messages for the Landsat data, the SPOT data, the airborne remote sensing data and other information, Mularz [7] explored the Belchatow lignite opencast mining area (Southwest Poland) comprehensively and extracted the changed data of the mining region by fusion of SPOT panchromatic in different time intervals. Tan et al. [8] summarized the methods and problems in the coal mine detection by using the remote sensing. Based on the multiple remote sensing messages of the Landsat5-TM data, Mao et al. [9] introduced a coal mine detection method which was used in Huozhou, Huolinhe and Pingshuo of China. Based on the remote sensing messages from the Landsat TM, the ETM data and the OLI data about the coal mining activities of Northern China, Li [10] proposed the evolution trend of the space and time of the coal mining activities which has become a reliable foundation for the local planning department as well as the environment department.

In recent years, the spectral characteristics have been successfully applied to many

scientific research fields. Body and Chadwick [11] used the laser-induced breakdown spectroscopy on lignite and measured the contents of some elements (i.e., Al, Si, Mg, Ca, Fe, Na, K, C, H etc.) based on the spectral data. Noda et al. [12] measured the coal fly ash carbon content based on the spectral characteristics. The fly ash carbon content was calculated by measuring the spectrum curves of the main elements such as Si, Al, Fe, Ca, C and so on. Dong, Lee, and Kim [13] addressed the coal quality problem based on the near infrared spectral analysis method. A predictive analytic model was established based on the multi-variable regression analysis, but it had about 10% prediction errors. Geng et al. [14] analyzed the carboxyl content of coal and coal aromaticity by the Fourier transform infrared spectrometry. The infrared reflection and transmission spectra analysis technology was used in the rapid detection of the coal quality by Bona and Andres [15]. The comprehensive analysis method based on the measured spectral data and the remote sensing data has been used in a lot of scientific research fields. Based on the measured spectral data and the remote sensing data, Quan et al. [16] proposed a soil water and salt content acquisition method. The method can timely obtain the improved effect of the salt lick area and the management condition of water resource. Based on the survey of the arctic field observation data and the satellite remote sensing data in 2012, Shi et al. [17] derived an algorithm by using the bright temperature data which was obtained from the ocean 2 satellite microwave scanning radiometer to inverse the ice concentration of Arctic sea. Based on the measured spectral data and the remote sensing data, Kuang, Luo, and Zhang [18] classified the water in the Boyang lake and developed a real-time monitoring method for it. In a word, a large number of studies have shown that the combination of the measured data and the remote sensing technology becomes very

promising in many fields.

Although the varieties of the remote sensors are increasing and the image resolution of the remote sensing is enhanced, the development of the analysis software has not been fully achieved. The accuracy of the traditional classification algorithms can hardly meet the actual requirements. The key issue is that if the satellite images are fast and accurate enough when an automatic classification of the remote sensing is used. In other words, an accurate and fast automatic classification of the satellite image has become a hot topic in the remote sensing field. To this end, this paper will introduce a new single hidden layer feedforward - Extreme Learning Machine (ELM), which is applied to construct a classifier for the remote sensing satellite image classification and can also be used as an approach to any complicated continuous functions. Most interestingly, its strong learning ability, fast training speed and high accuracy overcome some inherent shortcomings of the traditional neural networks.

In this paper, based on the spectral characteristics, an opencast coal mine exploration method has been developed by combining the measured spectral data with the spectral remote sensing data. The spectral data of the coal samples in Huolinhe and Quangninh are firstly measured by the spectrometer and then processed. Based on it, a more realistic surface reflectance and emissivity can be obtained. The coal image classification model was established based on the measured data and the remote sensing data. The model is used to classify the remote sensing images from the opencast coal mine in Huolinhe and Quangninh and pinpoint the distribution of the coal through the MATLAB simulation.

Moreover, the validity of the proposed method is confirmed by the application of the coal image classification model to another opencast coal region.

2. STUDY AREA AND DATA

2.1. Study Area

This study uses the coal mine area obtained from Huolinhe and Quangninh. Huolinhe is located in the eastern Inner Mongolia Autonomous Region of China. Its coalfield areas are 540 square kilometers and reserve 12.9 billion tons of lignite. It is also one of China's five full-surface coal mines with an annual production capacity of 10 million tons.

Vietnam's coal reserves are rich in variety and of good quality. Vietnam is one of the world's major coal-producing countries with Quangninh as a significant coal production base in the east of the country. Quangninh has large coal mines, with a mining history of over a century. The coalfield areas are 220 square kilometers and reserve 30 million tons of bituminite.

2.2. Pre-Processing Of The Measured Spectral Data

The lignite samples from Huolinhe and the bituminite samples from Quangninh have been obtained. Both coal samples are measured by the SVC HR-1024 portable feature spectrometer. The spectral range is 350-2500nm, with the weight of 3kg and 1024 channels. The spectral resolution: FWHM $\leqq$ 8.5nm and the minimum integration time is 1ms. Some coal samples are shown in Figure 1 (a) and the SVC HR- 1024 in Figure 1 (b).

The experiment is conducted between 10a.m and 2p.m under the sunshine with the solar altitude angle of 60 degrees (cloudless). The scanning time is 1 operation per second. The movement of the people should be avoided in order to reduce the change of the environment radiation. The surface of the coal samples should remain leveled; the lens of the spectrometer should be horizontal to the observation surface and also fit the observed direction of the earth satellite. Experimenters should wear dark color clothes in order to reduce the reflection as well as avoid the error caused by the experiment environment.

2.3. Pre-Processing Of The Satellite Data

The remote sensing images of the coal mining are downloaded from the USGS remote sensing image database. Landsat 8 is selected in this study, which is the most advanced satellite in the Landsat series and was launched on Feb 11st, 2013. It has two main loads: Operational Land Imager（OLI）and Thermal Infrared Sensor (TIRS).

OLI contains 9 wave bands, the spatial resolution is 30m, and the imaging width is 185x185km. OLI re-adjusts the wave bands in order to avoid absorption features, especially the OLI band 5 (0.845-0.885 μm) excludes the moisture absorption characteristics at 0.825μm. We only use the first seven wave bands because the Band 8 Pan and the Band 9 Cirrus are not in the scope of this research.

The original satellite image is vulnerable to the interference of the atmosphere and the surface reflectance of light thus the spectral data must be verified beforehand. Otherwise,

it may lead to distortion of the spectral data and geometry. ENVI is a powerful software for processing of the remote sensing image and is developed by American Exelis for Visual Information Solutions including the input/output image data, scaling, image enhancement, correction, mosaic, information extraction, image classification and so on. ENVI is used to eliminate the influence of the surface reflections from the atmosphere, light and other factors. A more realistic surface reflectance and emissivity, surface temperature and other physical model parameters can help to reflect the actual spectral characteristics of the ground substance. ENVI spectral calibration consists of the following two steps: radiometric calibration and atmospheric correction.

2.3.1. Radiometric Calibration

Radiometric calibration is a process of quantifying the value of voltage recorded by the sensor or converting digital number (DN) into absolute radiance value. ENVI 5.1 or the updated edition provides tools specifically for radiometric calibration of the Landsat8 satellite images.

Open the calibration band in the main menu, look up "/Radiometric Correction/Radiometric Calibration" in the toolbox, double-click this button, and choose the multispectral data which needs to be corrected. The requirement to Radiance data from FLAASH atmospheric correction is in the ".BIL" storage format. Get the relevant parameter by clicking Apply FLAASH settings, choose the output file name and finally click OK to execute the calibration.

2.3.2. Atmospheric Correction

ENVI contains a lot of atmospheric correction models. In this paper, the atmospheric correction is done by the MODTRAN model of the Landsat FLAASH. Since the parameters have already been set to meet the FLAASH atmospheric correction, now the FLAASH atmospheric correction tool can be directly used and there is no need to convert the data. Look up "/Radiometric Correction/Atmospheric Correction Module/FLAASH Atmospheric Correction" in the toolbox from ENVI 5.1 by double clicking this button. Open the data from Radiometric Calibration and perform the atmospheric correction according to the parameters including choosing the input and output files, the type of the satellite, the data of the images and so on.

It should be noted that the default wave band response function towards the Landsat 8 OLI in ENVI covers the cirrus wave band and the panchromatic wave band. Note that the cirrus wave band is located at the middle of the 7 panchromatic wave bands. It may cause a mistake if the wave band response function is used here, that is to say, all the results will be 0 after SWIR1 wave atmospheric correction. Therefore a new wave band response function has to be created to meet the 7 wave bands.

Figure 2 shows the results before and after the atmospheric correction. It can easily find the curve after atmospheric correction (as shown in Figure 2 (b)) since it is more like the real coal reflectance spectrum curve.

2.4. The Relationship Between Measured Data And Remote Sensing Data

There are 1024 wave bands in the SVC HR-1024 spectrometer during the spectral range of 350-2500nm. The 7 wave bands of the Landsat 8 OLI satellite are all covered by this spectrometer so we need to filter the measured data. Table 1 shows the corresponding relation between the 7 wave bands of the Landsat 8 OLI and the wave bands placed in the SVC HR-1024 spectrometer.

There is a comparison between the measured data and the remote sensing blackbody data, the result is shown in Figure 3. The blue dashed lines represent the remote sensing blackbody data which can reflect different substances on the ground. The red lines represent the coal measured data. It is quite clear that there are great differences between these two data during the 1st~5th wave band ranges. It is hard to distinguish the blackbody and the coal with the naked eyes. There will be a lot of wrong data if only the remote sensing data for sampling is used, which may cause unsatisfactory results. This is the main reason the measured data of spectra is used.

3. METHODS

3.1. Extreme Learning Machines

ELM is a simple and efficient learning algorithm for single- hidden layer feedforward neural networks (SLFNs) [19]. The aim of ELM is to solve the above issues related to the gradient-based algorithms. In an ELM, input weights and single hidden layer biases are arbitrarily chosen without iterative adjustments, and the only parameters to be learned in the training are the output weights which can be calculated by solving a single linear system [20]. Therefore, the ELM has been successfully applied to a great number of

problems, providing a good generalization performance at an extremely fast learning speed. N training samples can be defined, $\{\mathbf{X},\mathbf{T}\} = \{\mathrm{x}_j,\mathrm{t}_j\}_{j=1}^{N}$, where $x_j \in \mathbf{R}^p$ and $t_j \in \mathbf{R}^q$ are the $j-th$ input and target vectors, and the parameters p and q are the dimensions of the input and target vectors. To seek a regression function from the input to the target, one popular form is the standard single-hidden layer feedforward network (SLFNs) [21], where n_h single-hidden nodes fully connect the p input nodes to the q output nodes, which can be mathematically modeled as:

$$o_j = \sum_{i=1}^{n_h} \beta_i g(w_i^T x_j + b_i) = t_j, \qquad (1)$$

where $o_j \in \mathbf{R}^q$ is the output vector of the $j-th$ training sample, $w_j \in \mathbf{R}^p$ is the input weight vector connecting the input nodes to the $i-th$ hidden node, b_i is the bias of the $i-th$ hidden node, and $g(.)$ denotes the hidden nodes nonlinear piecewise continuous activation functions.

The above N equations can be written compactly as:

$$\mathbf{H}\beta = \mathbf{T}, \qquad (2)$$

where the matrix $\mathbf{T}$ is the target matrix,

$$\mathbf{H} = \begin{bmatrix} g\left(w_1^T x_1 + b_1\right) & \cdots & g\left(w_{n_h}^T x_1 + b_{n_h}\right) \\ \vdots & \cdots & \vdots \\ g\left(w_1^T x_N + b_1\right) & \cdots & g\left(w_{n_h}^T x_N + b_{n_h}\right) \end{bmatrix}, \qquad (3)$$

$$\beta = \begin{bmatrix} \beta_1^T \\ \vdots \\ \beta_{n_h}^T \end{bmatrix}, \quad \mathbf{T} = \begin{bmatrix} t_1^T \\ \vdots \\ t_N^T \end{bmatrix}. \qquad (4)$$

The matrix $\mathbf{H}$ is the hidden layer output matrix, which can be randomly generated independent of the training data. $\beta = [\beta_1, \beta_2, ..., \beta_{n_h}]^T$ $(\beta_i \in \mathbf{R}^q)$ is the output weighting matrix between the hidden nodes and the output nodes. Thus, to train the SLFNs simply amounts to solving the output weights β of a linear system (2) [22, 23].

According to the theoretical results in [24,25], an ELM aims to reach the smallest training error:

$$Minimize: \|\mathbf{H}\beta - \mathbf{T}\|. \qquad (5)$$

A simple representation of the solution of the equation (5) is given explicitly by Huang et al. [21] as follows:

$$\hat{\beta} = \mathbf{H}^{+}\mathbf{T}, \qquad (6)$$

where, $\mathbf{H}^{+}$ is the Moore-Penrose generalized inverse of the hidden layer output matrix $\mathbf{H}$.

3.2. Improved Extreme Learning Machines

In this neural network, the activation function plays a key role for the performance. If the selection of the activation function is inappropriate, then no matter how advanced the network structure and learning methods are, it is difficult to achieve satisfactory learning precision. Hornik, Stinchcombe, and White [26] and Leshno, Lin and Pinkus [27] have discussed about the performance of the additive node 'SLFN'. If the activation function is a bounded continuous non-constant polynomial, then it is sure to possess the ability to approach any continuous objective function. Moreover, if the activation function is chosen appropriately, the learning method will then play an important role.

Some of the common activation functions are as follows:

1. Sigmoid activation function, the function is defined as:

$$g(x)=\frac{1}{1+e^{-x}}. \qquad (7)$$

2. Rectified linear units (ReLU) activation function [28], the function is defined as:

$$g(x)=\max(0,x). \qquad (8)$$

3. Softplus activation function [29], the function is defined as:

$$g(x)=\ln(1+e^{x}). \qquad (9)$$

Sigmoid function is an effective threshold function and has great advantages in dealing with many existing problems. In recent years with the development of neural network deep learning, a novel linear ReLU correction function has been widely used, and gradually takes place of the Sigmoid activation function. ReLU function is much closer to the biology of the active model and has a simpler form. Since a ReLU does not use exponentiation and division, it has a much faster computing speed and also guarantees a good generalization performance. Recently, Glorot, Bordes [30] proposed an approximately smooth Softplus function, which is a much more powerful function than the Sigmoid function also because it is closely related to the biological model. Moreover, based on a large number of experiments, the literature [30] indicates that in general the Softplus function is better than the performance of the ReLU function. It is known that without a proper data preprocessing algorithm, the ReLU function will lead to infinite results in the calculation process, causing the whole system to break down.

In view of the above problems, this paper proposes a new activation function - logarithmic function (hereafter called Ln). The function is defined as:

$$g(x) = |\ln(x)|, \qquad (10)$$

The Ln activation function is a non-linear continuous differentiable function. It overcomes the shortcomings of the Softplus activation function. Plenty of experiments have confirmed the satisfactory performance of the Ln activation function.

In the ELM neural network, since the weights and bias are randomly given, the result of each output is unlikely to be the same. In view of challenge, we will integrate a large number of ELM sub-models to obtain an integrated ELM model. In this model, the test result of each sub-model is used to determine the final result. From the experiment results, 11 sub-models lead to the best performance. The accuracy of the integrated model is higher, and the running speed is faster. Our approach has 2 types of classification: the Class 1 and the Class 2. In the test results of these 11 sub-models, if the total number of the judgment result is greater than or equal to 6, then it can be considered that the end result is of the Class 1. The same procedure is also applicable for the Class 2. This method is called the "integrated ELM classification algorithm."

4. RESULTS AND VALIDATION: APPLICATION OF IMPROVED ELM ALGORITHM IN THE EXPLORATION OF COAL MINE AREAS

This study uses the data obtained from the lignite in Huolinhe and the bituminite in Quangninh. Among them there are 27 lignite samples and 21 bituminite samples. The measured data and the remote sensing satellite data are combined to create an image

classification model for these two mines. In this experiment, a comparison is made between the improved ELM algorithm with four different activation function neural networks (Sigmoid, ReLU, Softplus and Ln). The operating environment is as follows: Windows 7, Intel processor Pentium (R) Dual-Core E6700 @ 3.20GHz, 4GB RAM, NVIDIA GeForce 405 graphics plus, MATLAB 2014b.

An association between the ENVI software and the Google Earth Pro software is created. Thus, the ENVI software coal mine image latitude and longitude are mapped into the Google Earth Pro software from which we obtain the opencast coal mine ultra-HD resolution images (Google Images). Beforehand, the non-coal Google image area has been removed and only the coal zone is remained. Thus the obtained image is considered as the reference image.

4.1. Comparisons Of Results Obtained From The Matching Of Integrated ELM Model With The Different Activation Functions

4.1.1. Huolinhe Opencast Coal Mine Area

According to Figure 4, Figure 4(a), 4(b), 4(c) and 4(d) are the recognition model images of the Huolinhe coal mine area. The original image from the Landsat 8 satellite was taken in October 18th, 2015. Figure 4(e) is the reference image based on the Google Earth image. The original image was taken in August 3rd, 2015 (Figure 4(f)). The image recognition accuracies are shown in Table 2, it is concluded that the satellite image recognition method of the Huolinhe coal mine area has an accuracy of 97% or even more. The respective recognition accuracy rates of Softplus and Sigmoid function images are

97.4% and 97.76%. Ln activation function has the highest recognition accuracy which reaches 98.6%. That explains the impact of activation functions on ELM performance. The accuracy results have confirmed the effectiveness of the proposed method by using Ln as the activation function.

4.1.2. Quangninh Opencast Coal Mine Area

According to Figure 5, Figure 5(a), 5(b), 5(c), and 5(d) are the results of the Quangninh opencast coal mine recognition models. The original image from the Landsat 8 satellite was taken in January 18th, 2016. Figure 5 (e) is the reference image based on the Google Earth image. The original image was taken on the February 6th, 2016 (Figure 5(f)). The image recognition accuracies is shown are Table 3, it can be seen that the recognition accuracy of each method is higher than 90%. The Sigmoid activation function leads to the lowest recognition accuracy while the Ln activation function achieves the highest accuracy (95.4%). The results have further verified the merits of the Ln activation function.

4.2. Application Of The Coal Mine Exploration Model To Other Coal Mine Areas

Further tests will be carried out in this subsection. In the following, there will be an application on this method to two other mines, which are the Yimin opencast coal mine area in China and the Kalimantan Selatan opencast coal mine area in Indonesia.

According to Figure 6 and Figure 7, Figure 6(a) and Figure 7(a) are the results of the improved ELM recognition model for these two tests. The original images come from the

Landsat 8 satellite. Figure 6 (a) and Figure 7(a) were taken on July 5th, 2015 and July 24th, 2014 respectively. Figure 6 (b) and Figure 7(b) are downloaded and processed from Google Earth Pro software. Figure 8 (a) is the original image of Figure 6 (b), which was taken on July 7th, 2015; Figure 8 (b) is the original image of Figure 7 (b), which was taken on July 26th, 2014. The image recognition accuracies are shown in Table 4. When the method in this paper was applied in other coal mines, it is seen that the accuracies of the results are higher than 95%, which again proves the effectiveness of this method. The results indicate that the proposed approach is also applicable to other mines.

5. DISCUSSION: COMPARISON OF IMPROVED ELM ALGORITHM AND OTHER METHODS

In this section, there is a comparison between the proposed approach with some recent methods. Mao et al. [9] proposed a coal exploration method based on the Landsat 5 TM satellite data and the reflectance spectrum features (M-RSF). Thanks to this idea, the model of the Landsat 8 OLI in the following way is established.

Similar to the classic Normalized Difference Vegetation Index model (NDVI), a Normalized Difference Coal Index (NDCI) is presented in equation (11):

$$NDCI = \frac{OLI_6 - OLI_5}{OLI_6 + OLI_5}, \qquad (11)$$

where OLI_6 and OLI_5 are respectively the reflectance in bands 6 and 5 of the OLI image, which is obtained from the Landsat 8. Based on the analysis of the previous literature [9], the remote sensing image is finally obtained to extract the coal zone model.

$$\begin{cases} NDCI > a \\ b_1 < OLI_6 < b_2 \end{cases} \quad (12)$$

where a, b_1, and b_2 are obtained according to different types of coal.

Xiao et al. [31] proposed a coal exploration methods based on the pure remote sensing data (X-PRSD). Pure remote sensing data is obtained from the remote sensing image and taken directly as the sample data. This data is used to establish the classification model. It will inevitably lead to errors and inaccurate results.

Mao et al. [9] and Ferreira et al. [32] proposed the coal mine area recognition algorithms based on the random forest (RF). There is further comparision between the proposed approach with the above representative methods and the comparison results are shown in Figure 9, Figure 10 and Table 5.

According to Figure 9, it can be seen that the Quangninh coal mine area recognition accuracy rate is slightly lower because the Quangninh coal mine area is surrounded by many carbonaceous shale (Carbonaceous shale is a carbonaceous mixture of shale and sandy shale, carbonaceous 20% to 30%). Carbonaceous shale and coal spectral characteristics are similar thus the coal zone might contain a part of carbonaceous shale.

According to Table 5, in the Quangninh coal mine area, the improved ELM method possesses the highest accuracy while the RF method leads to the lowest accuracy. The results show that the proposed method is a better one.

In the Huolinhe coal mine area, Figure 10(a) shows the recognition image of the M-RSF

method. Some points of the lake, the building, the vegetation, etc have been mistaken as points of coal in Figure 10 (b) and Figure 10 (c). Figure 10 (d) shows the recognition image of the proposed improved ELM method. It is seen that the proposed method overcomes the shortcomings of the M-RSF, X-PRSD and RF methods. According to Table 5, it can be seen that the improved ELM method ensures the highest recognition accuracy, confirming the merits of the proposed approach.

Based on the differences in the images, it can be figured out that the errors are mainly caused by the following two issues. The first one is that the time satellite images and the Google image acquisition are not the same since the latter image is offered occasionally. The time of these images are made to be closer, but there still exist some differences. The second is the impact of carbonaceous shale. Coal and Carbonaceous shale quality spectral characteristics are similar, which cause some errors in the recognition model.

6. CONCLUSIONS

Remote sensing technology is playing an important role in all kinds of resource survey and prospecting process. It is an important technique for exploring the coal mining areas. In this study, the remote sensing, soft-sensing and spectra to the coal exploration. The data of the spectra of the coal and the remote sensing image of the mining area are collected. An improved ELM method is proposed to build the classification model. From the results, it's proved that the model can effectively separate the mining area image from the remote sensing image.

ACKNOWLEDGEMENTS

This research is supported by National Natural Science Foundation of China [Grant No. 41371437, 61203214], National Twelfth Five-Year Plan for Science and Technology Support [2015BAB15B01] PR China.

REFERENCES

[1] Bolch, T.; Menounos, B.; Wheate, R. LANDSAT-based Inventory of Glaciers in Western Canada, 1985–2005. *Remote Sensing of Environment* **2010**, 114 (1), 127-137.

[2] Hu, W.; Huang, Y. Y.; Wei, L.; et al. Deep convolutional neural networks for hyperspectral image classification. *Journal of Sensors* **2015**, 1, 1-12.

[3] Guo, C. F.; Guo, X. Y. Estimating leaf chlorophyll and nitrogen content of wetland emergent plants using hyperspectral data in the visible domain. *Spectroscopy Letters* **2015**, 49 (3), 180-187.

[4] Prakash, A.; Gupta, R. P. Land-use mapping and change detection in a coal mining area-a case study in the Jharia coalfield, India. *International Journal of Remote Sensing* **1998**, 19 (3), 391-410.

[5] Chen, H. L.; Chen, G.; Li, J. L.; et al. RS based ecological environmental dynamic monitoring in mining area. *Resources Science* **2004**, 26 (5), 132-138.

[6] Tian, F.; Wang, Y.; Fensholt, R.; et al. Mapping and evaluation of NDVI trends from synthetic time series obtained by blending Landsat and MODIS Data around a coalfield on the loess plateau. *Remote Sensing* **2013**, 5 (9), 4255-4279.

[7] Mularz, S. C. Satellite and airborne remote sensing data for monitoring of an open-cast mine. *IAPRS* **1998**, 32 (4), 395-402.

[8] Tan, K. L.; Wan, Y. Q.; Sun, S. X.; at al. Prospecting for coal in China with remote sensing. *Journal of China University of Mining & Technology* **2008**, 18 (4), 537-550.

[9] Mao, Y. C.; Ma, B. D.; Liu, S. J; et al. Study and Validation of a Remote Sensing Model for Coal Extraction Based on Reflectance Spectrum Features. *Canadian Journal of Remote Sensing* **2014**, 40 (5), 327-335.

[10] Li, N.; Yan, C. Z.; Xie, J. L. Remote sensing monitoring recent rapid increase of coal mining activity of an important energy base in northern China, a case study of Mu Us Sandy Land. *Resources Conservation and Recyclin*g **2015**, 94, 129-135.

[11] Body, D.; Chadwick, B. L. Simultaneous elemental analysis system using laser induced breakdown spectroscopy. *Review of Scientific Instrument* **2001**, 72 (3), 1625-1629.

[12] Noda, M.; Deguchi, Y.; Iwasaki, S.; et al. Detection of carbon content in a high-temperature and high-pressure environment using laser-induced breakdown spectroscopy. *Spectrochimica Acta Part B Atomic Spectroscopy* **2002**, 57 (4), 701-709.

[13] Dong, W. K.; Lee, J. M.; Kim, J. S. Application of near infrared diffuse reflectance spectroscopy for on-line measurement of coal properties. Korean Journal of Chemical Engineering **2009**, 26 (2), 489-495.

[14] Geng, W. H.; Nakajima, T.; Takanashi, H.; et al. Analysis of carboxyl group in coal and coal aromaticity by Fourier transform infrared (FT-IR) spectrometry. *Fuel* **2009**, 88 (1), 139–144.

[15] Bona, M. T.; Andres, J. M. Reflection and transmission mid-infrared spectroscopy for rapid determination of coal properties by multivariate analysis. *Talanta* **2008**, 74(4), 998–1007.

[16] Quan, Q.; Xie, J. C.; Shen, B.; et al. Soil sampling method based on field measurements and remote sensing images. *Transactions of the CSAE* **2010**, 26 (12), 237-241.

[17] Shi, L. J.; Lu, P.; Cheng, B.; et al. An assessment of arctic sea ice concentration retrieval based on "HY-2" scanning radiometer data using field observations during CHINARE-2012 and other satellite instruments. *Acta Oceanologica Sinica* **2015**, 34 (3), 42-50.

[18] Kuang, R. Y.; Luo, W.; Zhang, M. Optical classification of Poyang lake waters based on in situ measurements and remote sensing images. *Resources and Environment in the Yangtze Basin* **2015**, 24(5), 773-780.

[19] Huang, G. B.; Zhu, Q. Y.; Siew, C. K. Extreme learning machine: A new learning scheme of feedforward neural networks. *Proceedings of the 2004 IEEE International Joint Conference on, Neural Networks*, USA, July 25-29, 2004.

[20] Huang, G. B.; Zhou, H.; Ding, X.; et al. Extreme learning machine for regression and multiclass Classification. *IEEE Transaction on Systems, Man, and Cybernetics, Part B: Cybernetics* **2012**, 42(2), 513-529.

[21] Huang, G. B.; Zhu, Q. Y.; Siew, C. K. Extreme learning machine: Theory and applications. *Neurocomputing* **2006**, 70(1), 489-501.

[22] Feng, G.; Huang, G. B.; Lin, Q.; et al. Error minimized extreme learning machine with growth of hidden nodes and incremental learning. *IEEE Transactions on Neural Networks* **2009**, 20 (8),1352-1357.

[23] Huang,G. B. What are extreme learning machines? Filling the gap between Frank Rosenblatt's dream and John von Neumann's Puzzle. *Cognitive Computation* **2015**, 7(3), 263-278.

[24] Huang, G. B. An insight into extreme learning machines: Random neurons, random features and kernels. *Cognitive Computation* **2014**, 6 (3), 376-390.

[25] Cao, J. W.; Chen, T.; Fan, J. Y. Landmark recognition with compact BoW histogram and ensemble ELM. Multimedia Tools and Applications **2015**, 75 (5), 2839-2857.

[26] Hornik, K.; Stinchcombe, M.; White, H. Multilayer feedforward networks are universal approximators. Neural Networks **1989**, 2 (5), 359-366.

[27] Leshno, M.; Lin, V. Y.; Pinkus, A. Multilayer feedforward networks with a nonpolynomial activation function can approximate any function. *Neural Networks* **1993**, 6 (6): 861-867.

[28] Zeiler, M. D.; Ranzato, M.; Monga, R.; et al. On rectified linear units for speech processing. *Proceedings of the IEEE International Conference on Acoustics, Speech and Signal Processing*, USA, May 26-31, 2013.

[29] Zheng, H.; Yang, Z. L.; Liu, W. J.; et al. Improving deep neural networks using softplus units. *Proceedings of the International Joint Conference on Neural Networks*, IRELAND, July12-17, 2015.

[30] Glorot, X.; Bordes, A.; Bengio, Y. Deep sparse rectifier networks. *Journal of Machine Learning Research* **2011**, 15, 315-323.

[31] Xiao, D.; Le, B. T.; Mao, Y. C.; et al. Research on coal exploration technology based on satellite remote sensing. *Journal of Sensors* **2016**, 1, 1-9.

[32] Ferreira, M. P.; Zortea, M.; Zanotta, D. C.; et al. Mapping tree species in tropical seasonal semi-deciduous forests with hyperspectral and multispectral data. *Remote Sensing of Environment* **2016**,179, 66-68.

Table 1 The corresponding wave band relations of the Landsat 8 OLI and SVC HR-1024 sensors.

Band Name	Landsat 8-OLI (nm)	SVC HR-1024(nm)
1-Coastal	433–453	59(433.0)-72(452.7)
2-Blue	450–515	70(449.7)-114(515.5)
3-Green	525–600	120(524.4)-172(600.0)
4-Red	630–680	193(629.8)-229(679.9)
5- Near Infrared	845–885	358(845.5)-392(885.1)
6- Short-Wave Infrared 1	1560–1660	672(1558.2)-700(1659.7)
7- Short-Wave Infrared 2	2100–2300	857(2100.0)-937(2300.3)

Table 2 The accuracy rate of the coal exploration model's remote sensing image recognition of Huolinhe opencast coal mine based on different activation functions improved of ELM methods and visible-infrared spectra.

Activation function	Recognition accuracy
ReLU	97.04%
Softplus	97.40%
Sigmoid	97.76%
Ln	98.60%

Table 3 The accuracy rate of the coal exploration model's remote sensing image recognition of Quangninh opencast coal mine based on different activation functions improved of ELM methods and visible-infrared spectra.

Activation function	Recognition accuracy
Sigmoid	90.91%
ReLU	93.92%
Softplus	94.02%
Ln	95.41%

Table 4 The image recognition accuracy of other coal mine areas based on the coal mine area exploration model.

Coal mine areas	Recognition accuracy
Yimin	97.20%
Kalimantan Selatan	95.93%

Table 5 The image recognition accuracy of coal mine area of the different coal exploration methods used in Huolinhe and Quangninh opencast coal mine areas.

Methods	Huolinhe	Quangninh
M-RSF	96.53%	85.07%
X-PRSD	95.95%	89.77%
RF	96.02%	83.16%
Improved ELM	98.60%	95.41%

Figure 1 Pictures of some coal samples and the spectral measuring site: (a) Coal samples; (b) Spectral measuring site.

(a)

(b)

Figure 2 The comparison of coal's remote sensing spectral data of the before and after atmospheric correction: (a) before correction; (b) after correction.

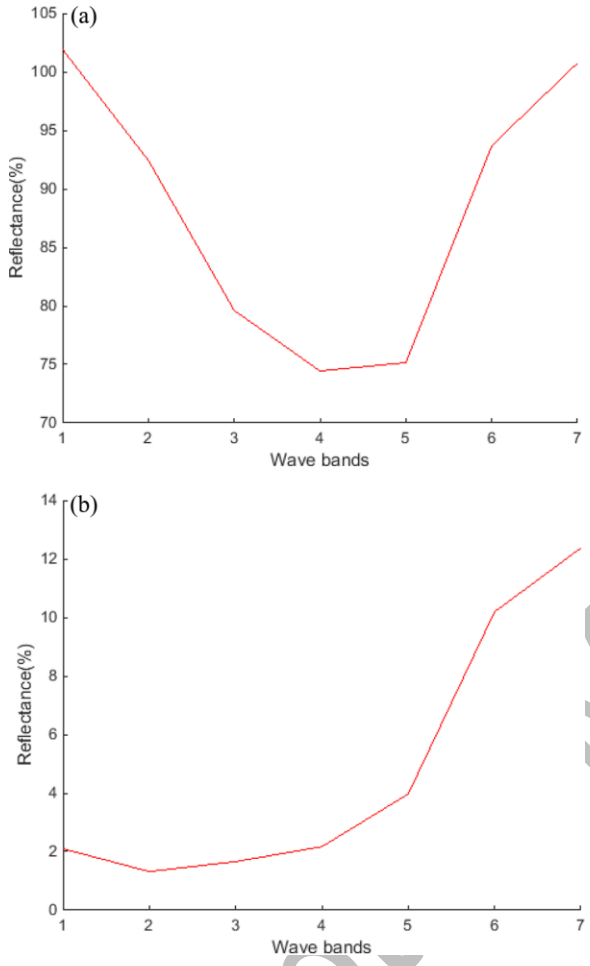

Figure 3 The comparison of the blackbody remote sensing spectral data and coal measured spectral data.

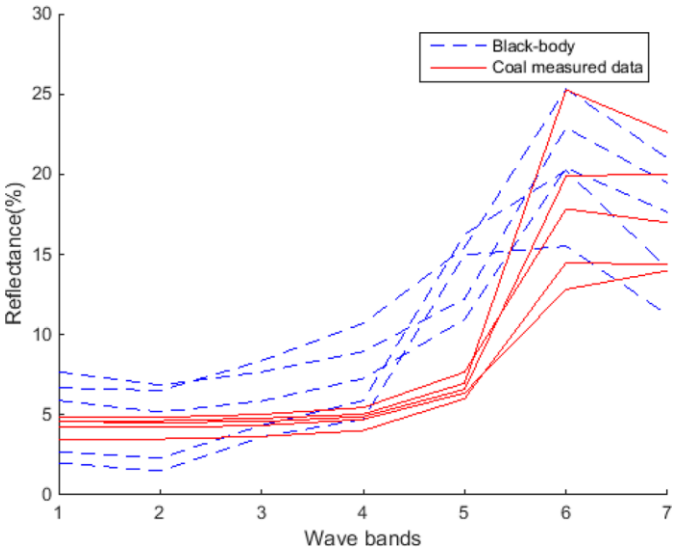

Figure 4 The coal exploration model's remote sensing image recognition of Huolinhe opencast coal mine based on different activation functions improved of ELM methods and visible-infrared spectra: (a) ReLU activation function; (b) Softplus activation function; (c) Sigmoid activation function; (d) Ln activation function; (e) Google image; (f) Google original image.

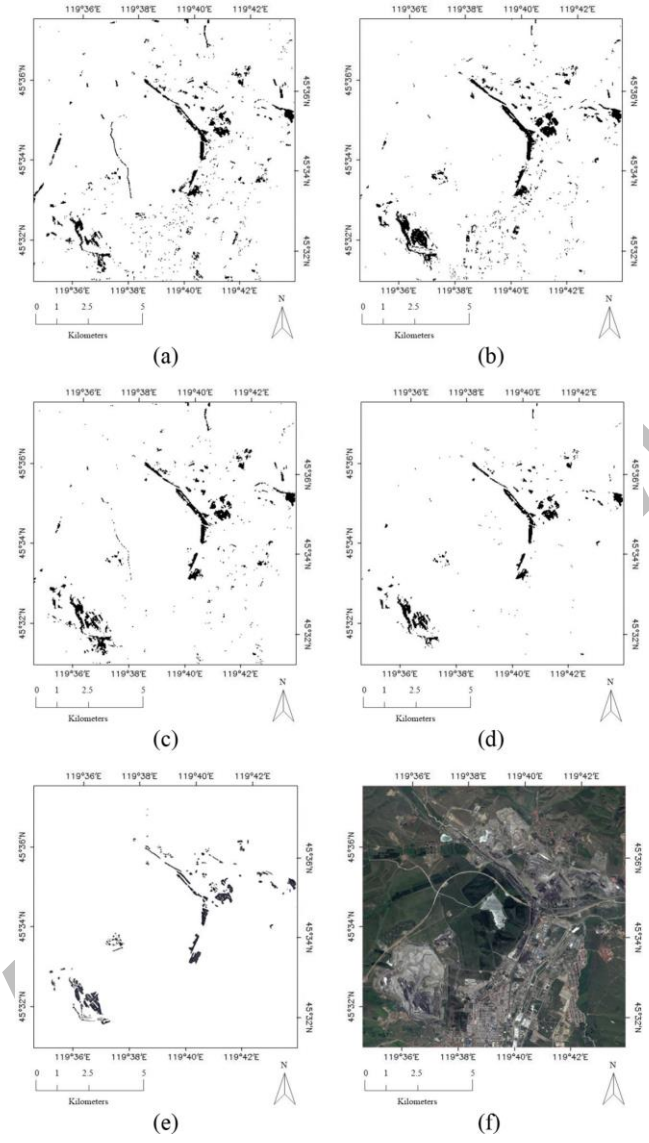

Figure 5 The coal exploration model's remote sensing image recognition of Quangninh opencast coal mine based on different activation functions improved of ELM methods and visible-infrared spectra: (a) ReLU activation function; (b) Softplus activation function; (c) Sigmoid activation function; (d) Ln activation function; (e) Google image; (f) Google original image.

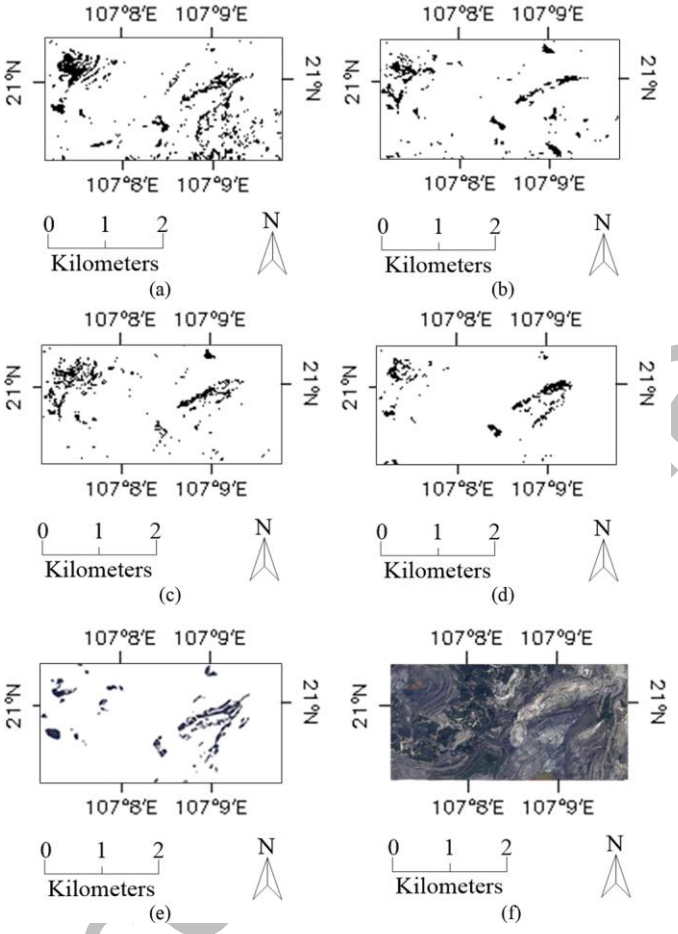

Figure 6 The remote sensing image recognition of Yimin coal mine based on the coal exploration model: (a) Improved ELM recognition model image; (b) Google image.

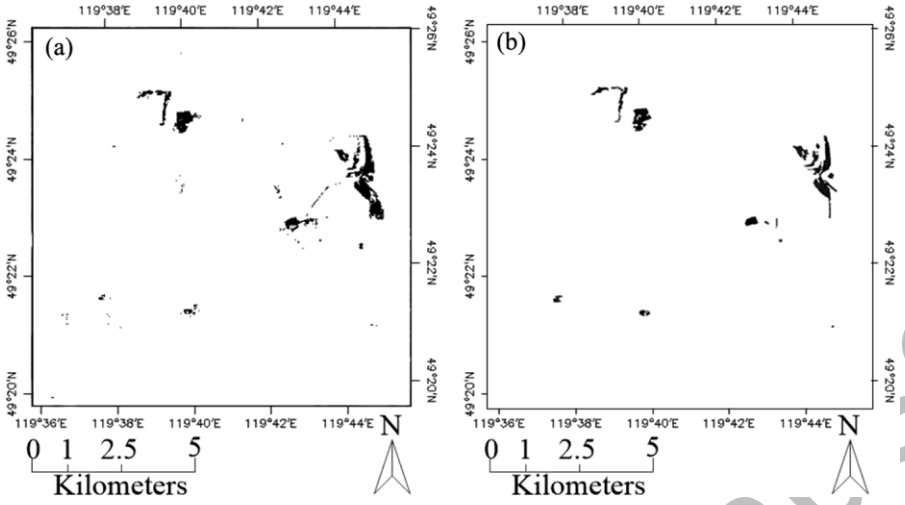

Figure 7 The remote sensing image recognition of Kalimantan Selatan coal mine based on the coal exploration model: (a) Improved ELM recognition model image; (b) Google image.

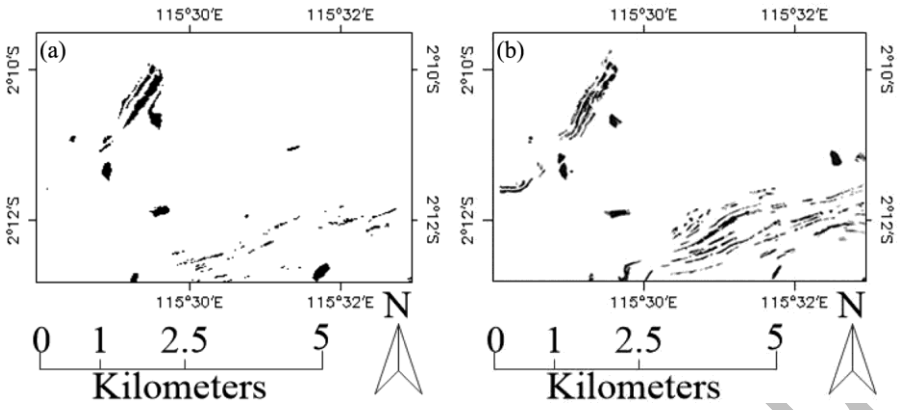

Figure 8 The Google original image of Yimin and Kalimantan Selatan opencast coal mine areas: (a) Yimin coal mine area; (b) Kalimantan Selatan coal mine area.

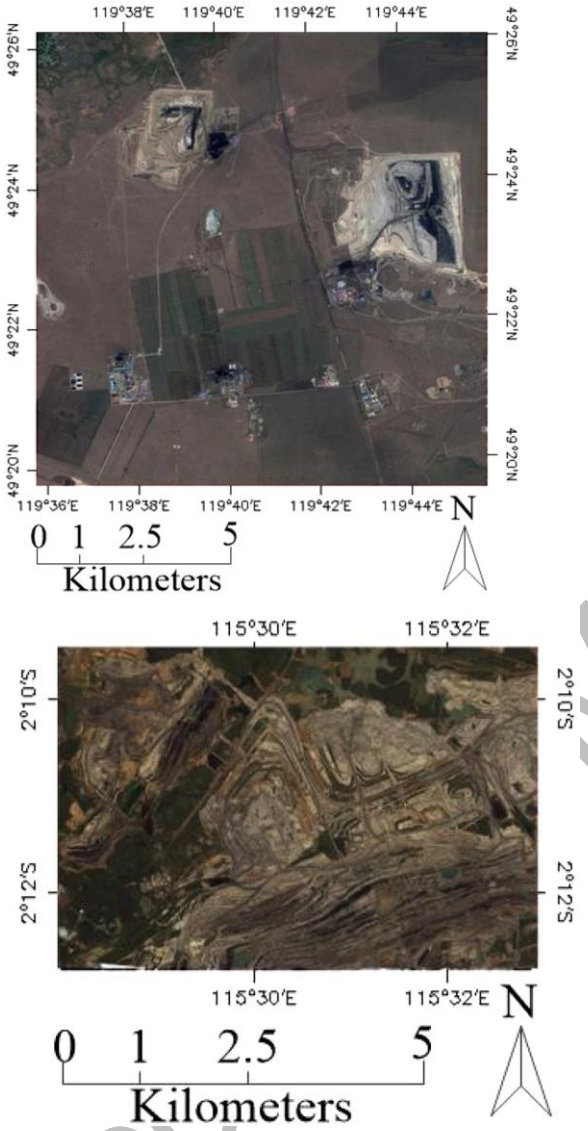

Figure 9 The Quangninh opencast coal mine remote sensing images for the different recognition coal exploration methods : (a) M-RSF method image; (b) X-PRSD method image; (c) RF method image; (d) Improved ELM method image; (e) Google image; (f) Google original image.

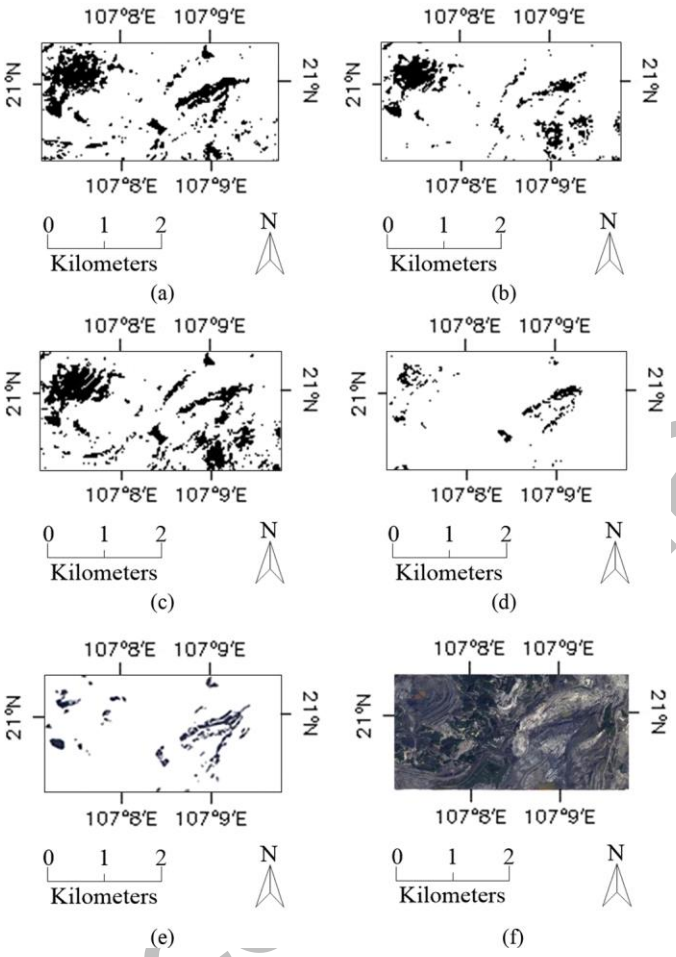

Figure 10 The Huolinhe opencast coal mine remote sensing images for the different recognition coal exploration methods: (a) M-RSF method image; (b) X-PRSD method image; (c) RF method image; (d) Improved ELM method image; (e) Google image; (f) Google original image.